Cu2O photoelectrodes for solar water splitting : tuning photoelectrochemical performance by controlled faceting

Solar Energy Materials & Solar Cells 141 (2015) 178–186

Contents lists available at ScienceDirect

Solar Energy Materials & Solar Cells

journal homepage: www.elsevier.com/locate/solmat

Cu_2O photoelectrodes for solar water splitting: Tuning photoelectrochemical performance by controlled faceting

Quan-Bao Ma *, Jan P. Hofmann, Anton Litke, Emiel J.M. Hensen *

Inorganic Materials Chemistry, Department of Chemical Engineering and Chemistry, Eindhoven University of Technology, P.O. Box 513, 5600 MB Eindhoven, The Netherlands

ARTICLE INFO

Article history:
Received 24 November 2014
Received in revised form
26 April 2015
Accepted 1 May 2015

Keywords:
Cu_2O films
Electrodeposition
pH effects
Water splitting
Photoelectrochemical properties
Solar energy

ABSTRACT

Cuprous oxide (Cu_2O) films were grown by electrodeposition in aqueous solutions of varying pH. The effect of bath pH on morphology, structural, and photoelectrochemical (PEC) properties of Cu_2O films was investigated. XRD showed that all prepared films were polycrystalline Cu_2O, without formation of competing phases such as CuO and Cu. The film grown in the solution with a pH of 8 is made up of Cu_2O crystallites with preferential (200) planes exposed. The films deposited at solution pH values of 10, 12 and 14 exhibit Cu_2O crystallites with preferential (111) planes exposed. As photoelectrodes these Cu_2O films generate photocurrent upon light illumination. The Cu_2O film grown in the solution with pH of 12 shows the best PEC performance for hydrogen generation. The (111) facets of the Cu_2O film were stable without corrosion during the PEC test. A mechanism for the preferred faceting in alkaline solution has been discussed.

1. Introduction

Photoelectrochemical (PEC) water splitting is a promising technology to produce renewable hydrogen with oxygen as a by-product from water and sunlight. Fujishima and Honda demonstrated PEC water splitting for the first time in 1972 using a TiO_2 photoelectrode [1]. Until now, materials such as $GaInP_2$ [2,3], Cu_2O [4–6], InGaN [7–10], InP [11], Fe_2O_3 [12] and SiC [13–15] have been used as photocathodes for PEC water splitting. Cu_2O is considered as one of the most promising photosensitive materials for PEC water splitting because of its low toxicity, abundance, good environmental acceptability and simple production process. Cu_2O is a p-type semiconductor with a direct band gap of 2.0 eV [4]. It can absorb solar radiation in the range of 300–620 nm, covering about 50% of the photons of the solar spectrum. Cu_2O is considered as a candidate photocathode in a PEC cell, because the conduction band edge of Cu_2O (ca. −1.35 V vs. Ag/AgCl at pH=7) is sufficiently more negative than the reduction potential of water (ca. −0.61 V vs. Ag/AgCl at pH=7) [16]. Therefore, Cu_2O is in principle capable of decomposing water into H_2 as a photocathode.

Cu_2O can be synthesized by various methods such as sputtering [17,18], chemical vapor deposition [19,20], thermal oxidation [21], chemical bath deposition [22], and electrodeposition [23–25]. Among them, the electrodeposition technique has attracted special interest for the preparation of Cu_2O thin films in recent years. It has two major advantages, namely its simplicity and the low growth temperature, leading to low cost processes and a large number of industrial applications. Also, electrodeposition allows control of the stoichiometry, thickness, and microstructure of the films by adjusting the deposition parameters. Until now there have been some reports on investigating the influence of pH on the preferred orientation of the Cu_2O crystallites that make up the film [26–28] but few mechanistic details were discussed.

In this work, electrodeposition was used to prepare Cu_2O films with different preferred crystal orientations. The effect of the pH of the bath on the morphology and the structural properties of the Cu_2O films was investigated. A growth mechanism of preferred faceting in alkaline solution as a function of pH taking into account the chemical speciation of Cu species in the bath was discussed. The (photo)electrochemical properties of the as-grown Cu_2O films were investigated in a 1 M Na_2SO_4 electrolyte in the dark and under light illumination. X-ray photoelectron spectroscopy (XPS) and scanning electron microscopy (SEM) measurements were carried out before and after the PEC tests to check the stability of the Cu_2O films against photocorrosion.

2. Experimental

Cu_2O films were electrodeposited in a two-electrode configuration in galvanostatic mode on fluorine-doped tin oxide (FTO) coated

* Corresponding author.
E-mail addresses: mqb7925921@163.com (Q.-B. Ma), e.j.m.hensen@tue.nl (E.J.M. Hensen).

http://dx.doi.org/10.1016/j.solmat.2015.05.025
0927-0248/

glass substrates. The substrate was cleaned with acetone and isopropanol, and subsequently rinsed with deionized water. A platinum sheet was used as a counter electrode. Cu_2O was electrodeposited by reduction of an alkaline aqueous solution of cupric lactate. The electrolytic bath contained 0.2–0.4 M copper(II) sulfate and lactic acid as chelating agent to stabilize Cu^{2+} ions by complexing. The bath temperature was set to 30–60 °C using a heating plate equipped with a temperature controller. The pH of the bath was adjusted to 8, 10, 12 or 14 by adding potassium hydroxide solution.

The as-deposited Cu_2O films were subjected to PEC evaluation in a dark-shielded box using a three-electrode configuration in a Teflon®-made PEC cell with a quartz glass window. The Cu_2O working electrode has an effective area of 0.5 cm^2. The counter electrode consisted of a Pt wire loop and the reference electrode Ag/AgCl in 3 M NaCl solution were used. A scanning potentiostat (controlled intensity modulated photo spectroscopy-CIMPS, Zahner) was used for the measurements of chopped light current-potential dependence. The illumination source used for PEC measurements was a Zahner LED (WLC02) white light source operated at a constant intensity of 1000 W/m^2. As electrolyte, aqueous 1.0 M Na_2SO_4 was used. The photoresponse measurements on chopped light voltammetry were performed for 3 scans before XPS observation. The scanning rate was 10 mV/s. For photostability tests, all the measurements were performed in 1 M Na_2SO_4 electrolyte solution with 0 V (vs. Ag/AgCl 3 M NaCl) bias applied for 24 h under light illumination.

The crystal structure of the films was analyzed by X-ray diffraction (XRD) using a Bruker D4 system with a Cu Kα source (λ=0.1541 nm). The film thickness and the surface morphology were determined using scanning electron microscopy (SEM)-XL30 and Quanta 3D FEG. XPS investigations were carried out on a Thermo Scientific K-Alpha system using an Al Kα (1486.6 eV) source for excitation.

3. Results and discussion

The pH of the electrolyte solution has a strong influence on the structure of electrodeposited Cu_2O films. X-ray diffraction patterns of Cu_2O films prepared from solutions of varying pH in the range of 8–14 are shown in Fig. 1. The thickness of all Cu_2O films as determined by SEM was around 1 μm. According to the XRD patterns, all prepared films are polycrystalline and can be indexed to the cubic Cu_2O phase with a lattice constant of a=4.252 Å. No other phases, in particular CuO and Cu, were detected by XRD. It was found that the film grown in the solution with pH=8 exhibited a pattern with strong Cu_2O peaks along the (200) axis, while the films deposited at higher pH had preferential orientation along the (111) axis, that is the (111) facets tend to be parallel to the substrate. These observations agree with results of Jeong et al. [29], reporting that the preferred facet of the Cu_2O film was (200) at pH lower than 9 and (111) at pH values higher than 10.

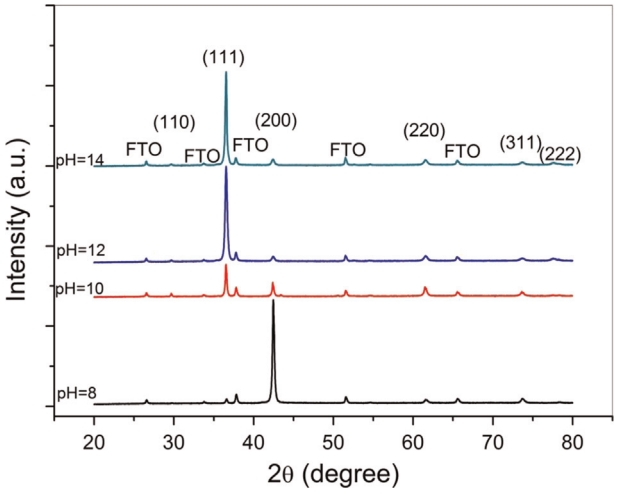

Fig. 1. X-ray diffraction patterns of Cu_2O films grown at different pH values.

To assess the quality of the as-deposited Cu_2O films, the full-width at half-maximum (FWHM) values of the (111) peaks were used to determine the crystallite size according to the Scherrer formula [30,31]. The FWHM and the grain size as a function of pH are shown in Fig. 2. With increasing pH, the crystallites of the Cu_2O films became larger. Fig. 2 shows that the average grain size along the (111) axis is between 29 and 46 nm. The film grown at pH=14 contains the largest crystallites. At a pH higher than 12, the plating solution became unstable and a milky precipitate formed. To prepare Cu_2O film with the preferential (111) facets the solution with pH=12 is preferred. It is suggested that the higher pH of the solution stimulates the grain growth of Cu_2O and forms films with large crystallites, therefore improve the crystallinity of Cu_2O films. Thus, the higher the pH, the larger the crystallites become. This phenomenon was also found in the experiments with electrodeposited Cu_2O by Gershon et al. [32].

Copper(II) ions in aqueous phase can form complex compounds with various organic and inorganic ligands. In this work a solution of $CuSO_4$ with lactate (LA) in the presence of KOH as a pH correcting agent is used for electrochemical deposition of Cu_2O on a conducting support. In this system two types of complexes can exist and/or coexist i.e. copper hydroxo-complexes $[Cu(OH)_n]^{2-n}$ and lactic complexes $[Cu(LA)_n]^{2-n}$. An attempt to assess the ionic composition of the solution at different pH has been done. In the following calculation the influence of the high ionic strength of the solution and possible deprotonation of the alpha-OH group of lactic acid at high pH values was not taken into account (pK_a(α-OH) ≈ 11 [33]).

The total formation constants of the lactate and hydroxo-complexes of Cu(II) are listed in Table 1.

At pH higher than 6.0 more than 99% of lactic acid in a solution is deprotonated (pK_a=3.86 [35]). Based on this the following equations

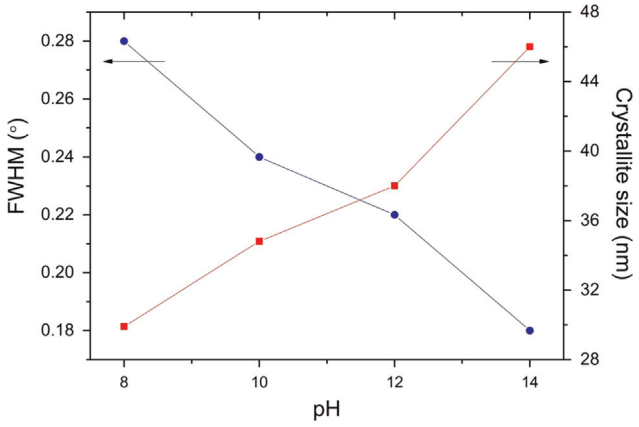

Fig. 2. Dependence of the FWHM and crystallite size on the bath pH for Cu_2O films.

Table 1
Total formation constants of Cu(II) complexes with different ligands[a].

Ligand	log β_1	log β_2	log β_3	log β_4
LA	3.02	4.85	–	–
OH^-	7.0	13.68	17.0	18.5

[a] Data were taken from Ref. [34]. Temperature for the listed values is between 20 and 25 °C. Values are given for zero ionic strength for OH^- and finite ionic strength for LA.

for the formation of the lactate complexes can be derived:

$$Cu^{2+} + LA^{-} \rightleftarrows [Cu(LA)]^{+} \quad (1)$$

$$[Cu(LA)]^{+} + LA^{-} \rightleftarrows [Cu(LA)_2]^{0} \quad (2)$$

$$Cu^{2+} + 2LA^{-} \rightleftarrows [Cu(LA)_2]^{0} \quad (3)$$

For the above listed reactions the equilibrium constants can be written as follows:

$$k_1 = \beta(LA)_1 = \frac{\{[Cu(LA)]^{+}\}}{\{Cu^{2+}\} \times \{LA^{-}\}}$$

$$k_2 = \frac{\beta(LA)_2}{\beta(LA)_1} = \frac{\{[Cu(LA)_2]^{0}\}}{\{[Cu(LA)]^{+}\} \times \{LA^{-}\}}$$

$$k_3 = \beta(LA)_2 = \frac{\{[Cu(LA)_2]^{0}\}}{\{Cu^{2+}\} \times \{LA^{-}\}^2}$$

where $\{A\}$ is an equilibrium concentration of species A, k_i is an equilibrium constant of the corresponding reaction and $\beta(N)_i$ is a total formation constant of a complex with i ligands of type N in the coordination sphere.

Besides, reactions (1)–(3) at high pH values following competing processes can take place:

$$Cu^{2+} + OH^{-} \rightleftarrows [Cu(OH)]^{+} \quad (4)$$

$$[Cu(OH)]^{+} + OH^{-} \rightleftarrows [Cu(OH)_2]^{0} \quad (5)$$

$$[Cu(OH)_2]^{0} + OH^{-} \rightleftarrows [Cu(OH)_3]^{-} \quad (6)$$

$$[Cu(OH)_3]^{-} + OH^{-} \rightleftarrows [Cu(OH)_4]^{2-} \quad (7)$$

$$Cu^{2+} + 4OH^{-} \rightleftarrows [Cu(OH)_4]^{2-} \quad (8)$$

$$k_4 = \beta(OH)_1 = \frac{\{[Cu(OH)]^{+}\}}{\{Cu^{2+}\} \times \{OH^{-}\}}$$

$$k_5 = \frac{\beta(OH)_2}{\beta(OH)_1} = \frac{\{[Cu(OH)_2]^{0}\}}{\{[Cu(OH)]^{+}\} \times \{OH^{-}\}}$$

$$k_6 = \frac{\beta(OH)_3}{\beta(OH)_2} = \frac{\{[Cu(OH)_3]^{-}\}}{\{[Cu(OH)_2]^{0}\} \times \{OH^{-}\}}$$

$$k_7 = \frac{\beta(OH)_4}{\beta(OH)_3} = \frac{\{[Cu(OH)_4]^{2-}\}}{\{[Cu(OH)_3]^{-}\} \times \{OH^{-}\}}$$

$$k_8 = \beta(OH)_4 = \frac{\{[Cu(OH)_4]^{2-}\}}{\{Cu^{2+}\} \times \{OH^{-}\}^4}$$

$$[Cu(LA)_2]^{0} + 2OH^{-} \leftrightarrow [Cu(LA)(OH)_2]^{-} + LA^{-} \quad (9)$$

$$[Cu(LA)(OH)_2]^{-} + 2OH^{-} \leftrightarrow [Cu(OH)_4]^{2-} + LA^{-} \quad (10)$$

$$[Cu(LA)_2]^{0} + 4OH^{-} \leftrightarrow [Cu(OH)_4]^{2-} + 2LA^{-} \quad (11)$$

$$k_9 = \frac{\{[Cu(LA)(OH)_2]^{-}\} \times \{LA^{-}\}}{\{[Cu(LA)_2]^{0}\} \times \{OH^{-}\}^2}$$

$$k_{10} = \frac{\{[Cu(OH)_4]^{2-}\} \times \{LA^{-}\}}{\{[Cu(LA)(OH)_2]^{-}\} \times \{OH^{-}\}^2}$$

and

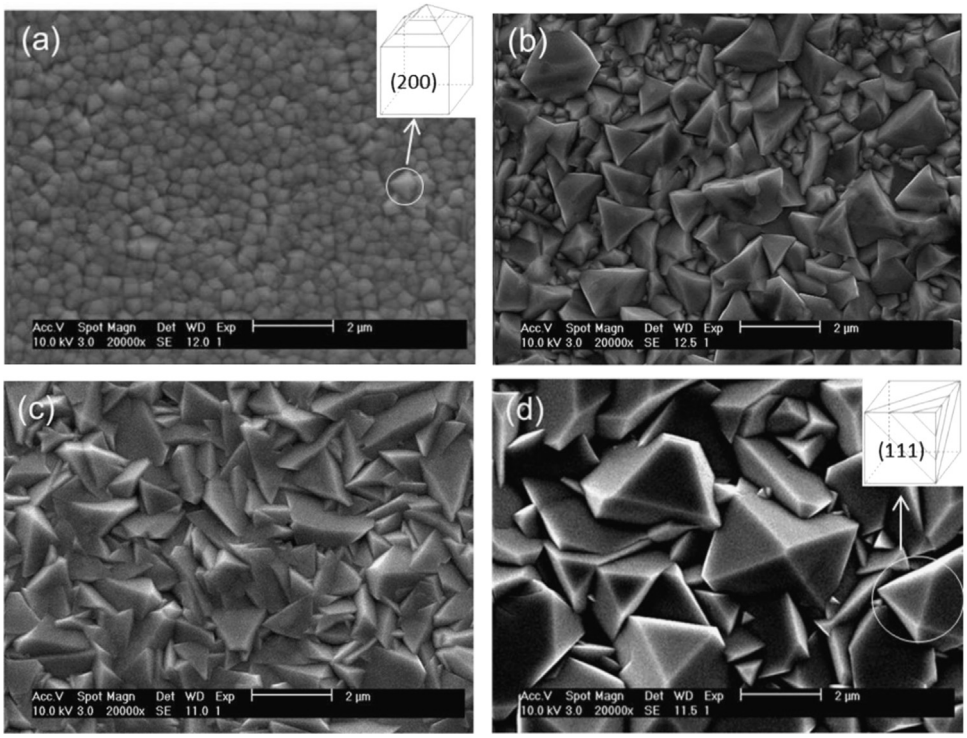

Fig. 3. SEM morphologies of Cu_2O films grown at different pH values: (a) pH=8; (b) pH=10; (c) pH=12; and (d) pH=14.

$$k_{11} = \frac{\{[Cu(OH)_4]^{2-}\} \times \{LA^-\}^2}{\{[Cu(LA)_2]^0\} \times \{OH^-\}^4} = \frac{\{[Cu(OH)_4]^{2-}\}}{\{Cu^{2+}\} \times \{OH^-\}^4} \times \frac{\{Cu^{2+}\} \times \{LA^-\}^2}{\{[Cu(LA)_2]^0\}} = \frac{\beta(OH)_4}{\beta(LA)_2}$$

To assess the ionic composition of the mixture at high pH values the reaction (11) and the equilibrium k_{11} can be used. The following simplification and assumptions are made to obtain an analytical expression for the dependence of the equilibrium concentration of metal complexes on the pH value:

(i) Reactions (1), (2), (4)–(7) and (10) are omitted based on the assumption that complexes $[Cu(LA)_2]^0$ and $[Cu(OH)_4]^{2-}$ are the predominant species. Reaction (9) is excluded from the calculation as formation constant of $[Cu(LA)(OH)_2]^-$ is unknown. So only processes (3), (8) and (11) are taken into consideration;

(ii) Based on the previous statement the material balance for lactate and copper can be written in the following formula:

$$c_\Sigma(Cu) = c_0(Cu^{2+}) = \{Cu^{2+}\} + \{[Cu(LA)_2]^0\} + \{[Cu(OH)_4]^{2-}\} \quad (12)$$

$$c_\Sigma(LA) = c_0(LA) = \{LA^-\} + 2 \times \{[Cu(LA)_2]^0\} \quad (13)$$

where $c_\Sigma(A)$ are the total concentrations of a compound A. The initial concentration $c_0(A)$ is known for every component and based on the amount of a corresponding substance added to the reaction mixture during the preparation.

Total concentrations of copper and lactate (lactic acid) are set as follows:

Taking into account the high values of the formation constants of the lactate and hydroxo-complexes of Cu(II) and the high initial concentration of the lactate anion and/or hydroxide (for the pH range above 10) it can be noticed that

$$\{Cu^{2+}\} << \{[Cu(LA)_2]^0\} + \{[Cu(OH)_4]^{2-}\}$$

That is, all copper(II) in solution are present in the form of complex compounds rather than in the form of hydrated Cu^{2+} cations. Accordingly, the formula (12) for Cu species can be rewritten as follows:

$$c_\Sigma(Cu) = c_0(Cu^{2+}) = \{[Cu(LA)_2]^0\} + \{[Cu(OH)_4]^{2-}\} \quad (14)$$

Based on the expressions (13) and (14) the following substitution can be done:

$\{[Cu(LA)_2]^0\} = x$,

$\{[Cu(OH)_4]^{2-}\} = c_0(Cu^{2+}) - x$

and

$\{LA^-\} = c_0(LA) - 2x$

The expression for k_{11} will be transformed into

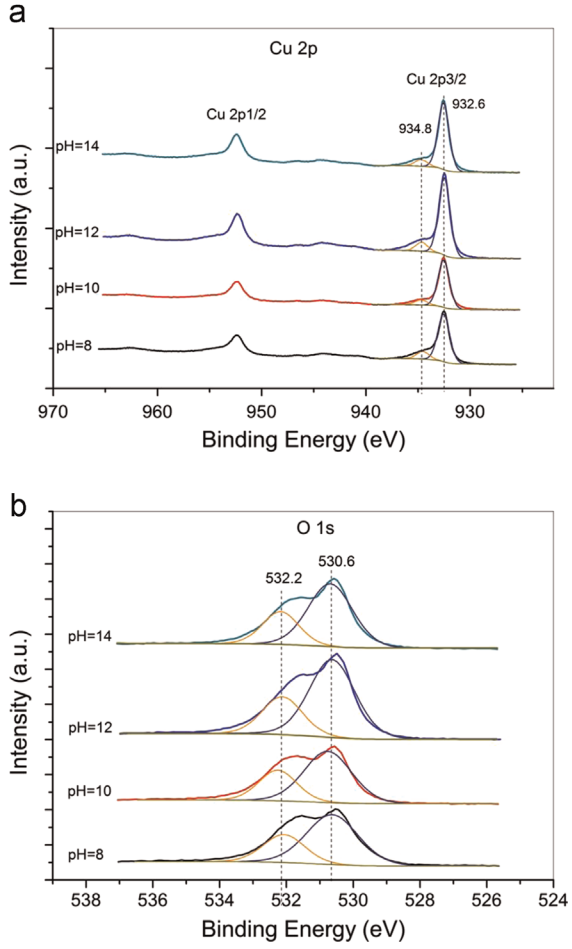

Fig. 4. X-ray photoelectron core level spectra of as-grown Cu_2O films: (a) Cu 2p peaks; and (b) O 1s peaks

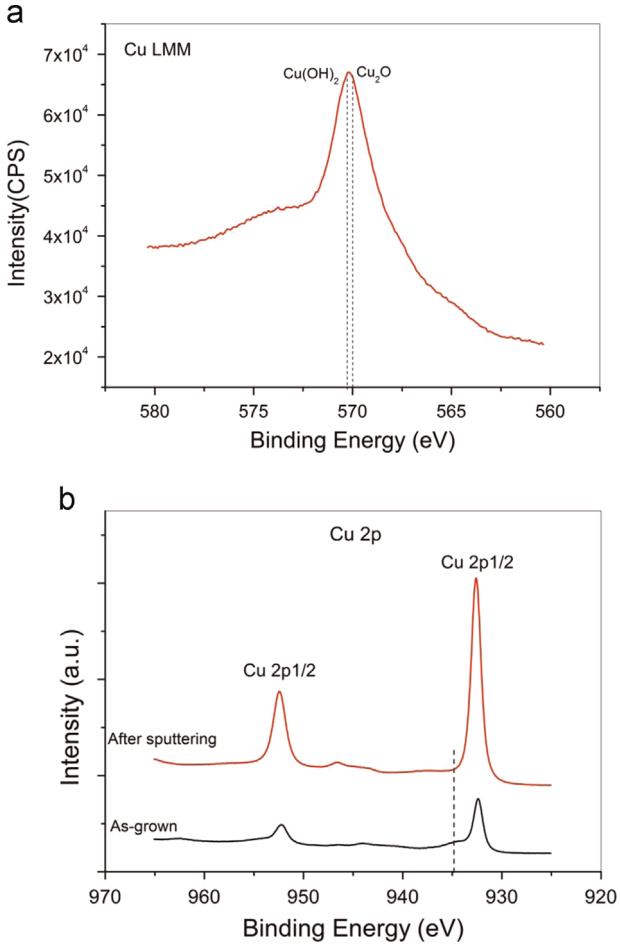

Fig. 5. (a) Binding energy data obtained for the Auger Cu LMM transition of the Cu_2O film grown at pH=12; (b) Cu 2p peaks before and after sputtering.

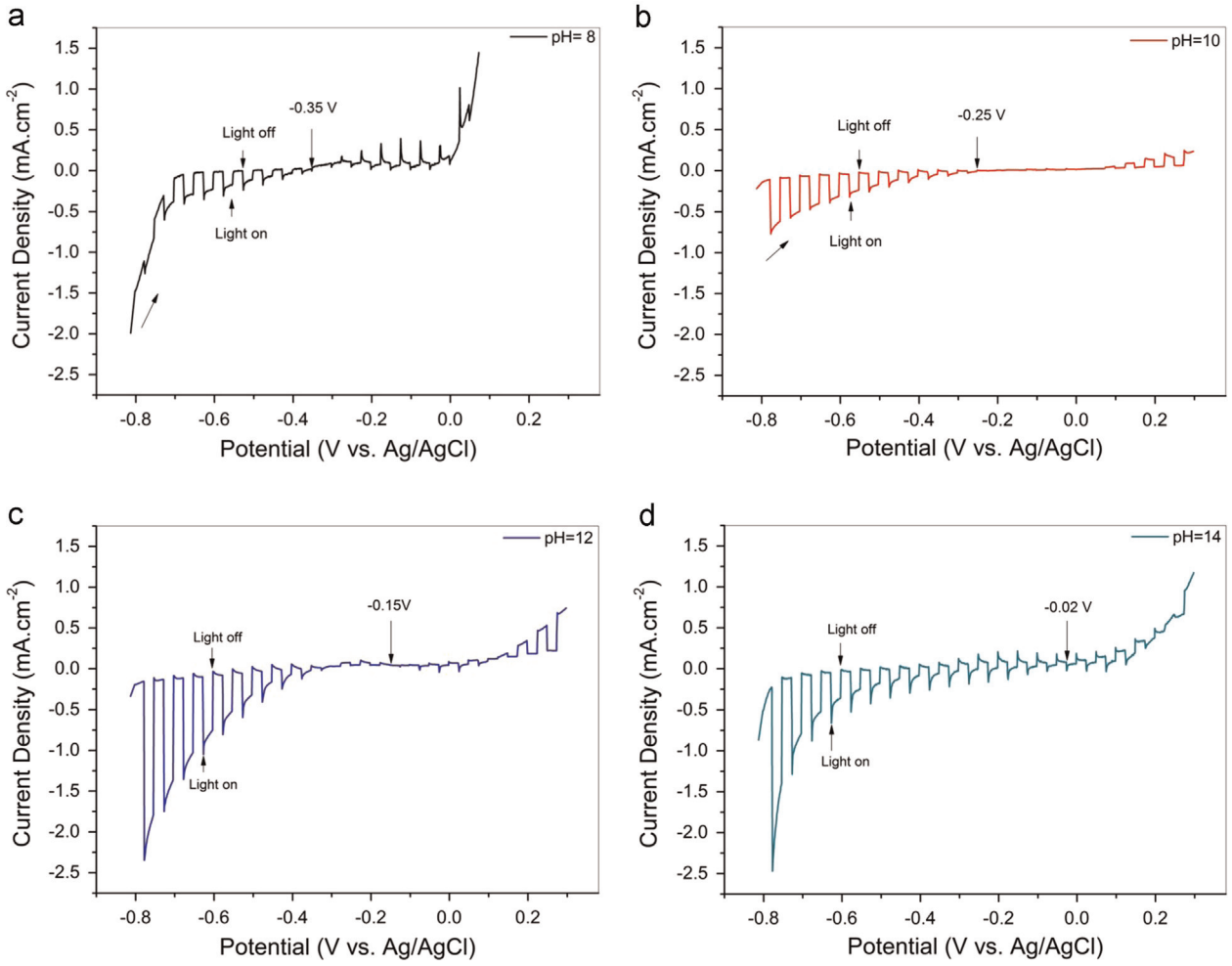

Fig. 6. Chopped current density–potential curves of Cu_2O films under light illumination: (a) pH=8; (b) pH=10; (c) pH=12; and (d) pH=14.

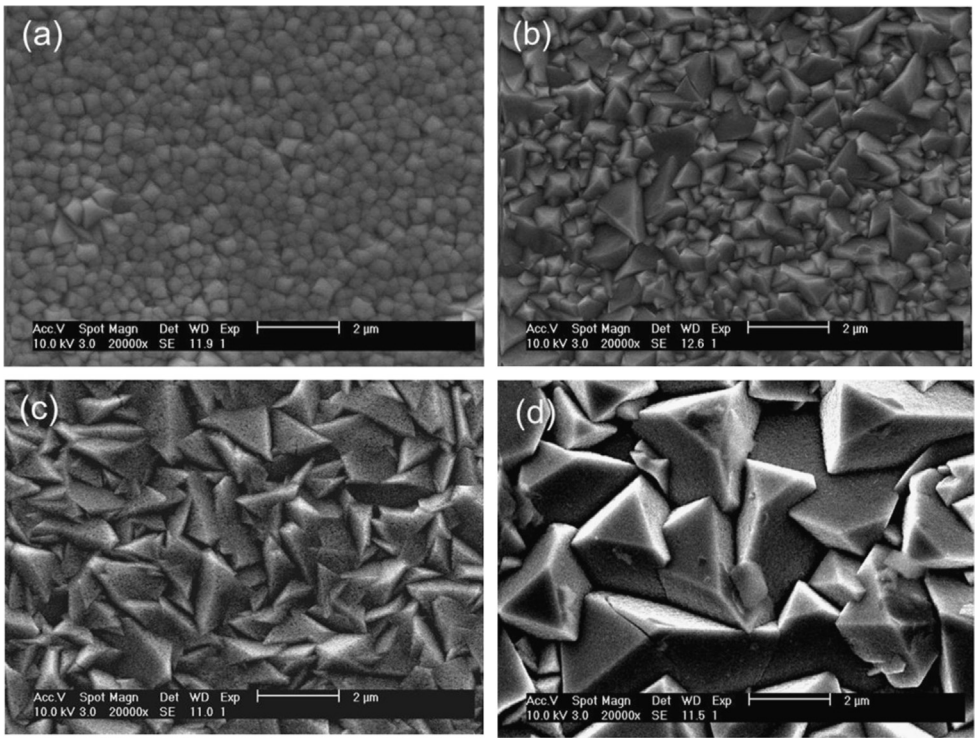

Fig. 7. SEM images of Cu_2O films after PEC tests: (a) pH=8; (b) pH=10; (c) pH=12; and (d) pH=14.

$$k_{11} = \frac{\beta(\mathrm{OH})_4}{\beta(\mathrm{LA})_2} = \frac{(c_0(\mathrm{Cu}^{2+}) - x) \times (c_0(\mathrm{LA}) - 2x)^2}{x \times \{\mathrm{OH}^-\}^4}$$

After simple algebraic transformation an equation can be obtained:

$$x^3 - x^2(c_0(\mathrm{Cu}^{2+}) + c_0(\mathrm{LA})) + 0.25x\left(4c_0(\mathrm{LA})c_0(\mathrm{Cu}^{2+}) + c_0(\mathrm{LA})^2 + \frac{\beta(\mathrm{OH})_4}{\beta(LA)_2}\{\mathrm{OH}^-\}^4\right) - 0.25c_0(\mathrm{Cu}^{2+})c_0(\mathrm{LA})^2 = 0 \quad (15)$$

A rough temperature correction of the equilibrium constants for the deposition conditions (T=50 °C) is made suggesting that ΔG does not depend on the temperature in the region 20–50 °C. The formation constant at temperature T_2 can be calculated based on the values known for T_1:

$$\Delta G = \mathrm{const} = \Delta G_1 = -RT_1 \ln K_1$$

$$K_2 = e^{-\frac{\Delta G}{RT_2}} = e^{\frac{T_1}{T_2}\ln K_1} = K_1^{\frac{T_1}{T_2}} \quad (16)$$

Eq. (16) is used to assess the composition of the reaction mixture. Corrected and uncorrected constants and initial concentrations of the reagents are used to solve the cubic Eq. (15) in the pH region 7–14 (the influence of the temperature on the pH is assumed to be negligible). Therefore, based on the formation constants of the Cu(II) complexes with different ligands (LA and OH^-), the ionic composition of the solution at different pH can be estimated (Fig. S1).

In the as-prepared alkaline solution the Cu(II) ions tend to form complex compounds with lactate and two types of complexes can exist, i.e. copper hydroxo-complexes $[Cu(OH)_n]^{2-n}$ and copper lactate-complexes $[Cu(LA)_n]^{2-n}$. The dependence of the $[Cu(LA)_2]$ concentration on the pH value of the reaction mixture (Fig. S1) indicates that at lower pH the solution mainly contains $[Cu(LA)_n]^{2-n}$, whereas at higher pH $[Cu(OH)_n]^{2-n}$ dominates. Accordingly, it is contended that $[Cu(OH)_n]^{2-n}$ facilitates the growth of Cu_2O crystals along the (111) axis and $[Cu(LA)_n]^{2-n}$ stimulates the Cu_2O growth along the (100) axis.

SEM images of the Cu_2O thin films grown in solutions of varying pH are shown in Fig. 3. The surface of the films is found to be continuous and dense. From the SEM images it can be seen that the film grows preferably in the (200) orientation in the solution with pH=8 in line with the XRD results. At pH=10 or higher the films increasingly tend to grow with preferred (111) orientation. Although the film deposited at pH=10 already shows a preferred (111) orientation in the XRD pattern, the film is composed of very small crystallites compared with those grown at pH values of 12 and 14. In a solution pH of 14, the largest crystallites are grown as can be seen also from the SEM images. The crystallites expose triangular (111) facets. In order to follow the crystal growth in time, Cu_2O was electrodeposited on FTO glass substrate at varying time. SEM analysis shows that initially uniform cubic crystals are formed with random orientation on the FTO substrate (Fig. S2). With increasing deposition time, the crystals grow preferably along the (111) axis (Figs. S2 and S3).

XPS was applied to investigate the chemical state of the surface of the Cu_2O films. XP Cu 2p and O 1s core level spectra are shown in Fig.4. The Cu 2p doublet exhibits an asymmetric shape with Cu $2p_{1/2}$ at 932.6 eV and Cu $2p_{3/2}$ at 952.4 eV. These positions are in accordance with other reports, where preferably Cu(I) oxide was grown by electrodeposition in alkaline solutions [36,37]. However, since Cu 2p features at these positions can in principle also be assigned to metallic Cu [38], the Cu LMM Auger transition in the XP spectrum was investigated as well. Fig. 5a shows the Cu LMM Auger spectrum of Cu_2O grown in the solution with pH=12 has a prominent peak around 570.0 eV. Metallic Cu would be expected in the binding energy range of 567.7–567.9 eV [39], while Cu_2O gives a signal at 570 eV and $Cu(OH)_2$ at 570.4 eV (at a similar position as Cu_2O) [40]. Fig. 5a confirms that the film consists of Cu_2O and possible $Cu(OH)_2$ and does not contain CuO. In order to confirm the existence of $Cu(OH)_2$ rather than CuO, the Cu_2O surface was sputtered in the XPS chamber and then re-analyzed by XPS. Fig. 5b shows the XP Cu 2p core level spectra measured before and after sputtering. It is found that the shoulder peak initially visible at the main Cu $2p_{3/2}$ feature had disappeared after sputtering, indicating only Cu^{2+} was present at the surface. It is known that exposure of Cu_2O to air will lead to formation of a Cu hydroxide surface contamination [39]. As the Auger peak for CuO is not developed in the spectra, it can be concluded that the shoulder peak of Cu $2p_{1/2}$ at 934.8 eV is due to $Cu(OH)_2$. Furthermore, $Cu(OH)_2$ signal corroborates possible mechanism of Cu^{2+} formation at higher pH's. So, from XPS and XRD the as-grown Cu-based oxide films are Cu_2O without formation of Cu or CuO, yet with minor contributions of $Cu(OH)_2$ at the surface.

Photoresponse measurements of the Cu_2O photocathodes were carried out by means of a potentiostat in a three-electrode setup with Ag/AgCl as the reference electrode and Pt as the counter electrode. The scanning rate was 10 mV/s. Fig. 6 shows the dependence of current density on the potential vs. Ag/AgCl under chopped light illumination for the Cu_2O films grown in the solutions of increasing pH. Fig. 6a–d shows that all Cu_2O films generate photocurrent when illuminated. The onset potentials of all electrodes are below 0 V vs. Ag/AgCl. The negative onset potential becomes smaller (less negative) for higher pH values of the chemical bath. For the Cu_2O film prepared at a pH of 8, the onset potential is at approximately −0.35 V vs. Ag/AgCl. When the applied potential is below this value, the electrode will generate a cathodic photocurrent. It can also generate a weak anodic photocurrent as a photoanode at higher than −0.35 V vs. Ag/AgCl. As it can start to generate the anodic photocurrent at more negative potential, it endured the oxidation on the surface much more than

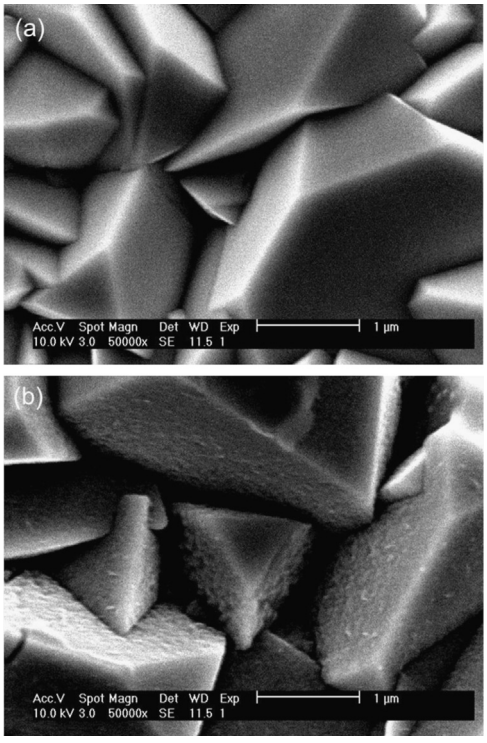

Fig. 8. SEM images of the Cu_2O film grown at pH=14 before and after PEC tests (magnification 50,000x).

other samples. Therefore, when it generated the anodic photocurrent, the surface would be oxidized even at more negative potential. The Cu_2O film grown at a pH of 12 shows the best PEC performance for hydrogen generation, as demonstrated by the highest photocurrent at a given potential. As a typical example for the PEC performance trend, the photocurrent density at −0.6 V decreased in the order (pH=12) > (pH=14) > (pH=10) > (pH=8).

After PEC measurements each sample was investigated by SEM to investigate possible changes on the morphology. Fig. 7 shows the representative SEM images of the tested Cu_2O films. XRD and SEM analysis of the composition, crystal morphology and crystallite sizes shows that no significant changes have taken place. Compared with Fig. 3, the only clear change in the SEM images is the appearance of dots on certain crystal planes. In Fig. 8, the film grown at a pH of 14 is displayed at higher magnification before and after PEC measurements, indicating a pronounced roughening of the (200) facets. In contrast, the (111) facets of the Cu_2O film remained unchanged with at least at this scale no obvious changes due to light illumination in the electrolyte.

Contrasting the reported surface energies of the (111) surface (−212.39 eV) and (200) surface (−215.25 eV) from first-principles DFT calculations [41], the Cu_2O (111) surface is the more stable one and Cu_2O (200) surface the most active. Different crystal facets possess different surface energy levels of conduction and valence bands [41]. Compared with the Cu_2O (111) facet, the valence band of Cu_2O (200) is known to be shifted to higher energies. Accordingly, it is surmised that photogenerated holes will move to higher energy facets such as (200) facets. At the same time, photogenerated electrons will preferentially move to energetically favorable (111) facets. Accordingly, it may be speculated that the oxidation reaction mainly takes place on the (200) facets and the reduction on the (111) facets. It is then reasonable to state that the (200) facets will be oxidized more easily than the (111) facets by an anodic photocurrent, which would deteriorate the PEC performance of the film terminated by predominantly (200) facets.

After PEC measurements, XPS was applied again to investigate changes in chemical surface composition and oxidation state of Cu of the Cu_2O electrodes. The survey spectrum confirmed that the O emission for Cu_2O film (pH=8) is considerably increased after PEC experiments, whereas Cu 2p emission is decreased (Figs. S4 and S6), indicating that the films had been oxidized. XP core level spectra of Cu and O for all Cu_2O films after PEC measurements are shown in Fig. 9. For the sample grown at the pH of 8, the Cu $2p_{3/2}$ peak is fitted into two peaks: one at 932.6 eV and the other one at 934.7 eV. The peak at 932.6 eV is attributed to Cu_2O, while the

Table 2
Binding energy, FWHM and contribution of Cu $2p_{3/2}$ peaks after PEC measurements.

pH	Binding energy (eV)		FWHM (eV)		Contribution (%)	
	Cu^+	Cu^{2+}	Cu^+	Cu^{2+}	Cu^+	Cu^{2+}
8	932.6	934.7	1.22	2.49	37.5	62.5
10	932.5	934.9	1.73	1.44	83.4	16.6
12	932.6	934.7	1.49	1.46	84.4	15.6
14	932.4	934.5	1.26	1.50	88.1	11.9

Table 3
Binding energy, FWHM and contribution of O 1s peaks after PEC measurements.

pH	Binding energy (eV)		FWHM (eV)		Contribution (%)	
	Cu_2O	$Cu(OH)_2$	Cu_2O	$Cu(OH)_2$	Cu_2O	$Cu(OH)_2$
8	530.6	531.7	1.14	1.50	20.1	79.9
10	530.7	532.3	1.68	1.50	70.8	29.2
12	530.7	532.1	1.46	1.33	71.6	28.4
14	530.2	531.7	1.79	1.49	73.4	26.6

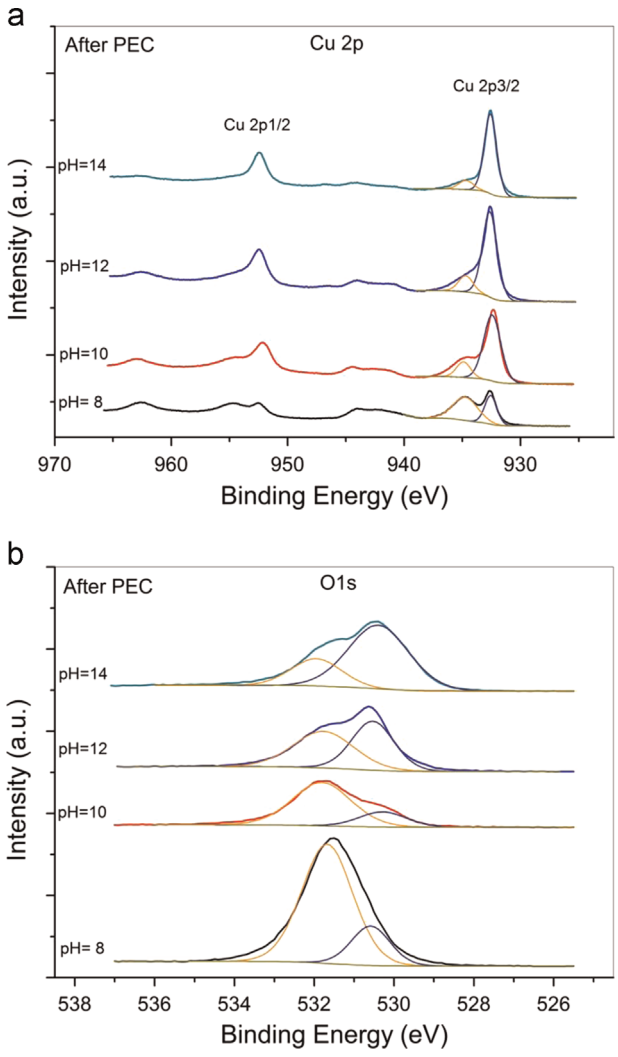

Fig. 9. X-ray photoelectron core level spectra of Cu_2O films after PEC tests: (a) Cu 2p peaks; and (b) O 1s peaks.

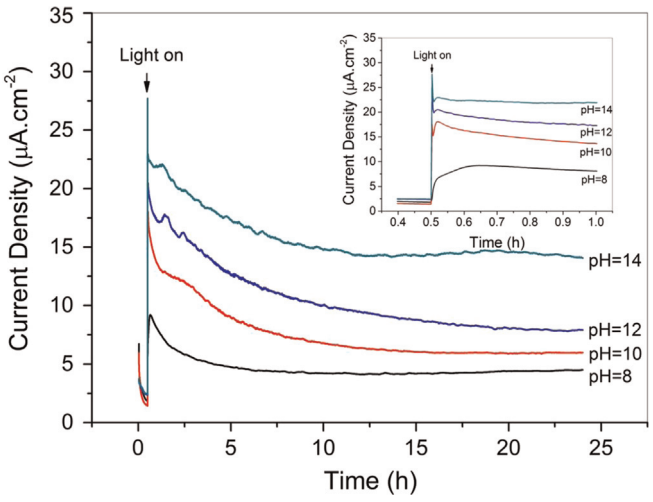

Fig. 10. Dependence of current density on time for photostability tests of Cu_2O films.

peak at 934.7 eV attributed to $Cu(OH)_2$, indicating that the Cu_2O on the surface was partly oxidized into $Cu(OH)_2$ under the anodic photocurrent during the PEC measurement. The fitting results of Cu $2p_{3/2}$ peaks for all the samples are listed in Table 2. The intensity of the $Cu(OH)_2$ peaks decreased with increasing bath pH. At pH=14, the shoulder peak of Cu $2p_{3/2}$ due to $Cu(OH)_2$ has the lower contribution (11.9%) among all films characterized after PEC measurements. Two component fitting of the O 1s peaks shows contributions from Cu_2O and $Cu(OH)_2$. The fitting results of the O 1s peaks are listed in Table 3. The O 1s core level spectra reveal that the Cu_2O film grown at the pH of 8 was oxidized to a larger degree during PEC tests than the films grown at higher pH.

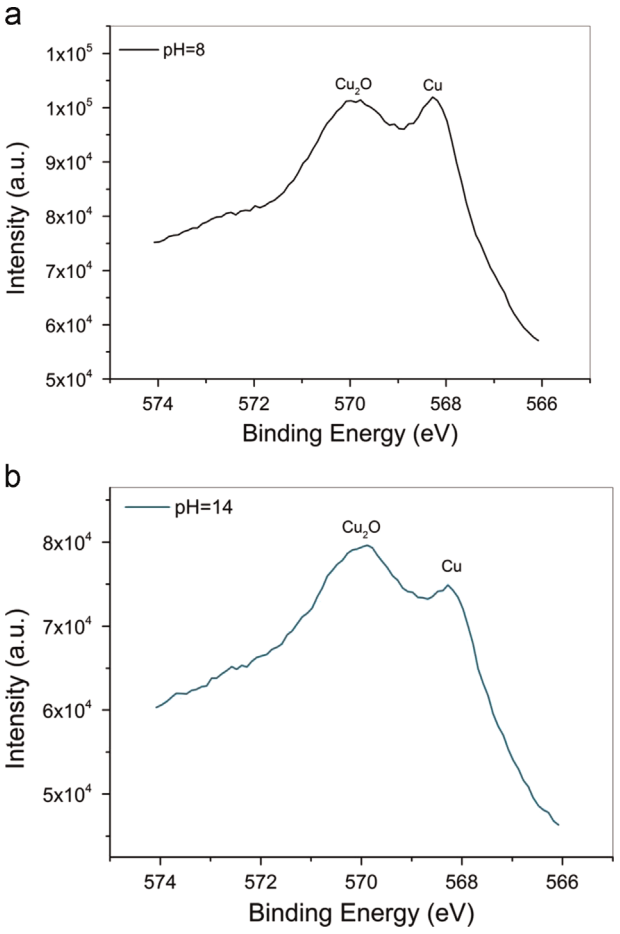

Fig. 11. Auger Cu LMM transition of Cu_2O films after the photostability tests of 24 h: (a) pH=8; (b) pH=14.

The photostability tests on the synthesized Cu_2O films were performed in 1 M Na_2SO_4 electrolyte solution with 0 V (vs. Ag/AgCl 3 M NaCl) bias applied for 24 h under light illumination. The dependence of current density on time is showed in Fig. 10, indicating that the film grown at higher pH can generate more photocurrent for water splitting at 0 V and the photocurrent for all the films can still be observed after 24 h although the current decreased due to the photocorrosion. For the Cu_2O film grown at pH=8, after the light on the photocurrent was increased slowly on the beginning due to the film photo-dissolution, as showed in the inset in the Fig. 10. Compare with other samples the photocurrent of the Cu_2O film with preferable (111) facets grown at pH=14 stayed almost on the same level with the light on in 30 min. But for the film grown at pH=8, some small spots were exposed with no film on the electrode after 24 h due to the severe photocorrosion. The photostability tests showed that the film growth at pH=14 still has the photoactivity of over 60% left after 24 h while the film grown at pH=8 just around 45% left.

The Auger measurements in Fig. 11 show that the Cu_2O on the surface of the electrodes was partly reduced to Cu metal after 24 h of the photostability tests and the film grown at pH=8 endured severe corrosion more than that grown at pH=14 observed from the relative intensity of Cu_2O and Cu peak. It also indicates that Cu_2O was still existed on the electrodes even after 24 h of the photostability tests. From the SEM morphologies in Fig. 12. It can be seen that the surface of the film with preferable (002) facets was corroded heavily while the surface on the film with preferable (111) facets still showed the smooth (111) facets, indicating that the (111) facets are more stable than (002) facets for solar water splitting.

4. Conclusions

Cu_2O films were grown by electrodeposition in aqueous lactacte solutions of varying pH. The effect of bath pH on morphology, structural and photoelectrochemical properties of Cu_2O films was investigated. XRD patterns showed that all as-prepared films are polycrystalline, and, except for Cu_2O, no other phases, such as CuO and Cu, could be detected. The film grown at pH=8 showed Cu_2O peaks with preferential orientation along (200) axis and films deposited at pH values of 10, 12 and14 exhibited Cu_2O peaks with preferential orientation along (111) axis. ($[Cu(OH)_n]^{2-n}$) complexes present at higher alkaline pH promote the Cu_2O growth along (111) axis and ($[Cu(LA)_n]^{2-n}$) complexes stimulate the Cu_2O growth along (200) axis.

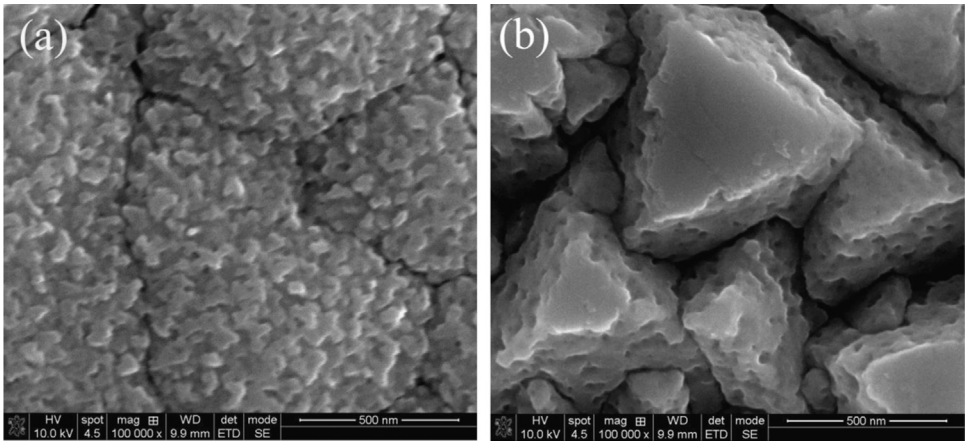

Fig. 12. SEM morphologies of Cu_2O films after the photostability tests of 24 h: (a) pH=8; and (b) pH=14.

The average grain size along the (111) axis for the as-prepared films is found to be between 29 and 46 nm. The film grown at pH = 14 has the narrowest FWHM and thus the largest crystallites. Cu 2p shows a doublet peak with an asymmetric shape: Cu $2p_{1/2}$ at 932.6 eV and Cu $2p_{3/2}$ at 952.4 eV attributed to Cu_2O. SEM images also showed that the films grew with preferable (200) orientation in lower pH solution. At pH ≥ 10 the films started to grow with preferable (111) orientation. All Cu_2O films can generate photocurrent during light illumination. The PEC performance of Cu_2O can be tuned by controlled faceting. The Cu_2O film grown in the solution pH = 12 showed the best PEC performance for hydrogen generation. The photostability tests showed that the film grown at pH = 14 still has the photoactivity of over 60% left after 24 h but the film grown at pH = 8 just around 45% left. The (111) facets of the Cu_2O film are more stable than other facets for solar water splitting.

Acknowledgments

The authors gratefully acknowledge Mrs. Yi Zhang for the assistance with SEM measurements, Mr. Ad Wonders and Mr. Johan J.G. van Velzen for support during the experiments, and Mr. M.W.G.M.(Tiny) Verhoeven for XPS training and the assistance on XPS measurments.

Appendix A. Supplementary material

Supplementary data associated with this article can be found in the online version at http://dx.doi.org/10.1016/j.solmat.2015.05.025.

References

[1] A. Fujishima, K. Honda, Electrochemical photolysis of water at a semiconductor electrode, Nature 238 (1972) 37–38.
[2] O. Khaselev, J.A. Turne, Electrochemical stability of p-$GaInP_2$ in aqueous electrolytes toward photoelectrochemical water Splitting, J. Electrochem. Soc. 145 (1998) 3335–3339.
[3] H. Wang, J.A. Turner, Stability of $GaInP_2$ in H_2SO_4 solution for photoelectrochemical water splitting, ECS Trans. 27 (2007) 125–133.
[4] J.N. Nian, C.C. Hu, H. Teng, Electrodeposited p-type Cu_2O for H_2 evolution from photoelectrolysis of water under visible light illumination, Int. J. Hydrog. Energy 33 (2008) 2897–2903.
[5] S. Somasundaram, C.R.N. Chenthamarakshan, N.R. de Tacconi, K. Rajeshwar, Photocatalytic production of hydrogen from electrodeposited p-Cu_2O film and sacrificial electron donors, Int. J. Hydrog. Energy 32 (2007) 4661–4669.
[6] R.M. Liang, Y.M. Chang, P.W. Wu, P. Lin, Effect of annealing on the electrodeposited Cu_2O films for photoelectrochemical hydrogen generation, Thin Solid Films 518 (2010) 7191–7195.
[7] K. Aryal, B.N. Pantha, J. Li, J.Y. Lin, H.X. Jiang, Hydrogen generation by solar water splitting using p-InGaN photoelectrochemical cells, Appl. Phys. Lett. 96 (2010) 052110.
[8] J. Li, J.Y. Lin, H.X. Jiang, Direct hydrogen gas generation by using InGaN epilayers as working electrodes, Appl. Phys. Lett. 93 (2008) 162107.
[9] Q.B. Ma, R. Lieten, G. Borghs, Effects of annealing on the structural properties of indium rich InGaN films, J. Mater. Sci. Mater. Electron. 25 (2014) 1197–1201.
[10] Q.B. Ma, R. Lieten, S. Degroote, M. Germain, G. Borghs, Indium-rich InGaN films grown on Ge substrate by plasma-assisted molecular beam epitaxy for solar water splitting, J. Electron. Mater. 44 (2015) 202–209.
[11] M.H. Lee, K. Takei, J. Zhang, R. Kapadia, M. Zheng, Y.Z. Chen, J. Nah, T.S. Matthews, Y.L. Chueh, J.W. Ager, A. Javey, p-Type InP nanopillar photocathodes for efficient solar-driven hydrogen production, Angew. Chem. Int. Ed. 51 (2012) 10760–10764.
[12] W.B. Ingler Jr., S.U.M. Khan, Photoresponse of spray pyrolytically synthesized copper-doped p-Fe_2O_3 thin film electrodes in water splitting, Int. J. Hydrog. Energy 30 (2005) 821–827.
[13] Q.B. Ma, B. Kaiser, J. Ziegler, D. Fertig, W. Jaegermann, XPS characterization and photoelectrochemical behaviour of p-type 3C–SiC films on p-Si substrates for solar water splitting, J. Phys. D: Appl. Phys. 45 (2012) 325101.
[14] Q.B. Ma, J. Ziegler, B. Kaiser, D. Fertig, W. Calvet, E. Murugasen, W. Jaegermann, Solar water splitting with p-SiC film on p-Si: photoelectrochemical behavior and XPS characterization, Int. J. Hydrog. Energy 39 (2014) 1623–1629.
[15] Q.B. Ma, B. Kaiser, W. Jaegermann, Novel photoelectrochemical behaviors of p-SiC films on Si for solar water splitting, J. Power Sources 253 (2014) 41–47.
[16] C.-C. Hu, J.N. Nian, H. Teng, Electrodeposited p-type Cu_2O as photocatalyst for H_2 evolution from water reduction in the presence of WO_3, Sol. Energy Mater. Sol. Cells 92 (2008) 1071–1076.
[17] H. Zhu, J. Zhang, C. Li, F. Pan, T. Wang, B. Huang, Cu_2O thin films deposited by reactive direct current magnetron sputtering, Thin Solid Films 517 (2009) 5700–5704.
[18] W.Y. Yang, W.G. Kim, S.W. Rhee, Radio frequency sputter deposition of single phase cuprous oxide using Cu_2O as a target material and its resistive switching properties, Thin Solid Films 517 (2008) 967–971.
[19] S. Eisermann, A. Kronenberger, A. Laufer, J. Bieber, G. Haas, S. Lautenschläger, G. Homm, P.J. Klar, B.K. Meyer, Copper oxide thin films by chemical vapor deposition: synthesis, characterization and electrical properties, Phys. Status Solidi A 209 (2012) 531–536.
[20] T. Maruyama, Copper oxide thin films prepared by chemical vapor deposition from copper dipivaloylmethanate, Sol. Energy Mater. Sol. Cells 56 (1998) 85–92.
[21] J. Liang, N. Kishi, T. Soga, T. Jimbo, M. Ahmed, Thin cuprous oxide films prepared by thermal oxidation of copper foils with water vapor, Thin Solid Films 520 (2012) 2679–2682.
[22] P.B. Ahirraoa, B.R. Sankapalb, R.S. Patil, Nanocrystalline p-type-cuprous oxide thin films by room temperature chemical bath deposition method, J. Alloy. Compd. 509 (2011) 5551–5554.
[23] M. Izaki, T. Shinagawa, K.T. Mizuno, Y. Ida, M. Inaba, A. Tasaka, Electrochemically constructed p-Cu_2O/n-ZnO heterojunction diode for photovoltaic device, J. Phys. D: Appl. Phys. 40 (2007) 3326–3329.
[24] Z. Xi, H. Zeng, N. Liao, L. Shi, H. Huang, S. Guo, N. Wang, D. Jin, L. Wang, Study on the effect of annealing on the electrical properties of n-type cuprous oxide, Thin Solid Films 520 (2012) 2708–2710.
[25] A. Paracchino, V. Laporte, K. Sivula, M. Grätzel, E. Thimsen, Highly active oxide photocathode for photoelectrochemical water reduction, Nat. Mater. 10 (2011) 456–461.
[26] A. Paracchino, J.C. Brauer, J.-E. Moser, E. Thimsen, M. Graetzel, Synthesis and characterization of high-photoactivity electrodeposited Cu_2O solar sbsorber by photoelectrochemistry and ultrafast spectroscopy, J. Phys. Chem. C 116 (2012) 7341–7350.
[27] C. Jayewardena, K.P. Hewaparakrama, D.L.A. Wijewardena, H. Guruge, Fabrication of n-Cu_2O electrodes with higher energy conversion efficiency in a photoelectrochemical cell, Sol. Energy Mater. Sol. Cells 56 (1998) 29–33.
[28] C.A.N. Fernando, S.K. Wetthasinghe, Investigation of photoelectrochemical characteristics of n-type Cu_2O films, Sol. Energy Mater. Sol. Cells 63 (2000) 299–308.
[29] S.S. Jeong, A. Mittiga, E. Salza, A. Masci, S. Passerini, Electrodeposited ZnO/Cu_2O heterojunction solar cells, Electrochim. Acta 53 (2008) 2226–2231.
[30] Q.B. Ma, Z.Z. Ye, H.P. He, S.H. Hu, J.R. Wang, L.P. Zhu, Y.Z. Zhang, B.H. Zhao, Structural, electrical, and optical properties of transparent conductive ZnO:Ga films prepared by DC reactive magnetron sputtering, J. Cryst. Growth 304 (2007) 64–68.
[31] Q.B. Ma, Z.Z. Ye, Y. Luo, L.P. Zhu, Y.Z. Zhang, B.H. Zhao, Highly infrared reflective behavior of transparent conductive ZnO:Ga films synthesized by DC reactive magnetron sputtering, ChemPhysChem 9 (2008) 529–532.
[32] T.S. Gershon, N.N. Lal, J.J. Baumberg, J.L. MacManus-Driscoll, Tunable Mie scattering from electrodeposited Cu_2O nanoparticles, J. Electrochem. Soc. 159 (2012) D747–D749.
[33] R. Portanova, L.H.J. Lajunen, M. Tolazzi, J. Piispanen, Critical evaluation of stability constants for alpha-hydroxycarboxylic acid complexes with protons and metal ions and the accompanying enthalpy changes, Pure Appl. Chem. 75 (2003) 495–540.
[34] J.A. Dean, Lange's Handbook of Chemistry, 14th ed.,. McGraw-Hill, London, 1992.
[35] D.R. Lide (Ed.), CRC Handbook of Chemistry and Physics, CRC Press, Boca Raton, FL, 2005.
[36] C. Zhu, A. Osherov, M.J. Panzer, Surface chemistry of electrodeposited Cu_2O films studied by XPS, Electrochim. Acta 111 (2013) 771–778.
[37] J. Morales, L. Sanchez, S. Bijani, L. Martinez, M. Gabas, J.R. Ramos-Barradob, Electrodeposition of Cu_2O: an excellent method for obtaining films of controlled morphology and good performance in Li-ion batteries, Electrochem. Solid-State Lett. 8 (2005) A159–A162.
[38] Y. Mao, J. He, X. Sun, W. Li, X. Lu, J. Gan, Z. Liu, L. Gong, J. Chen, P. Liu, Y. Tong, Electrochemical synthesis of hierarchical Cu_2O stars with enhanced photoelectrochemical properties, Electrochim. Acta 62 (2012) 1–7.
[39] T. Waechtler, S. Oswald, N. Roth, A. Jakob, H. Lang, R. Ecke, S.E. Schulz, T. Gessner, A. Moskvinova, S. Schulze, M. Hietschold, Copper oxide films grown by atomic layer deposition from bis(tri-n-butylphosphane)-copper(I) acetylacetonate on Ta, TaN, Ru, and SiO_2, J. Electrochem. Soc. 156 (2009) H453–H459.
[40] Z. Duan, A.D. Pasquier, Y. Lu, Y. Xu, E. Garfunkel, Effects of Mg composition on open circuit voltage of Cu_2O–$Mg_xZn_{1-x}O$ heterojunction solar cells, Sol. Energy Mater. Sol. Cells 96 (2012) 292–297.
[41] Z. Zheng, B. Huang, Z. Wang, M. Guo, X. Qin, X. Zhang, P. Wang, Y. Dai, Crystal faces of Cu_2O and their stabilities in photocatalytic reactions, J. Phys. Chem. C 113 (2009) 14448–14453.